Using optoacoustic imaging for measuring the temperature dependence of Grüneisen parameter in optically absorbing solutions

Elena Petrova,* Sergey Ermilov, Richard Su, Vyacheslav Nadvoretskiy, André Conjusteau, and Alexander Oraevsky

TomoWave Laboratories, Inc., 6550 Mapleridge St., Suite 124, Houston, Texas 77081, USA
**ep@tomowave.com*

Abstract: Grüneisen parameter is a key temperature-dependent physical characteristic responsible for thermoelastic efficiency of materials. We propose a new methodology for accurate measurements of temperature dependence of Grüneisen parameter in optically absorbing solutions. We use two-dimensional optoacoustic (OA) imaging to improve accuracy of measurements. Our approach eliminates contribution of local optical fluence and absorbance. To validate the proposed methodology, we studied temperature dependence of aqueous cupric sulfate solutions in the range from 22 to 4°C. Our results for the most diluted salt perfectly matched known temperature dependence for the Grüneisen parameter of water. We also found that Grüneisen-temperature relationship for cupric sulfate exhibits linear trend with respect to the concentration. In addition to accurate measurements of Grüneisen changes with temperature, the developed technique provides a basis for future high precision OA temperature monitoring in live tissues.

OCIS codes: (170.5120) Photoacoustic imaging; (120.6780) Temperature; (120.6810) Thermal effects.

References and links

1. A. A. Oraevsky and A. A. Karabutov, "Optoacoustic tomography," in *Biomedical Photonics Handbook*, T. Vo-Dinh, ed. (CRC, 2003), pp. 34/31–34/34.
2. L. V. Wang and S. Hu, "Photoacoustic tomography: in vivo imaging from organelles to organs," Science **335**(6075), 1458–1462 (2012).
3. B. Cox, J. G. Laufer, S. R. Arridge, and P. C. Beard, "Quantitative spectroscopic photoacoustic imaging: a review," J. Biomed. Opt. **17**(6), 061202 (2012).
4. S. Manohar, T. G. van Leeuwen, J. M. Klaase, F. M. van den Engh, and W. Steenbergen, "Photoacoustic mammography with a flat detection geometry," in *Photoaccoustic Imaging and Spectroscopy*, L. V. Wang, ed. (CRC, 2009), pp. 431–442.
5. A. A. Oraevsky, "Optoacoustic tomography of the breast," in *Photoaccoustic Imaging and Spectroscopy*, L. V. Wang, ed. (CRC, 2009), pp. 411–429.
6. S. Sethuraman, B. Wang, R. Smalling, and S. Emelianov, "Intravascular photoacoustic imaging of atherosclerosis," in *Photoaccoustic Imaging and Spectroscopy*, L. V. Wang, ed. (CRC, 2009), pp. 451–461.
7. G. J. Diebold, "Photoacoustic monopole radiation: waves from objects with symmetry in one, two, and three dimensions," in *Photoaccoustic Imaging and Spectroscopy*, L. V. Wang, ed. (CRC, 2009), pp. 3–17.
8. V. E. Gusev and A. A. Karabutov, *Laser Optoacoustics* (AIP, 1993).
9. A. A. Oraevsky, S. L. Jacques, and F. K. Tittel, "Measurement of tissue optical properties by time-resolved detection of laser-induced transient stress," Appl. Opt. **36**(1), 402–415 (1997).
10. N. Bilaniuk and G. S. K. Wong, "Speed of sound in pure water as a function of temperature," J. Acoust. Soc. Am. **93**(3), 1609–1612 (1993).
11. D. Eisenberg and W. Kauzmann, *The Structure and Properties of Water (Oxford Classic Texts in the Physical Sciences)* (Oxford University, 2005).
12. L. G. Hepler, "Thermal expansion and structure in water and aqueous solutions," Can. J. Chem. **47**(24), 4613–4617 (1969).

#195773 - $15.00 USD Received 27 Aug 2013; revised 4 Oct 2013; accepted 4 Oct 2013; published 14 Oct 2013

13. L. Talley, G. Pickard, W. Emery, and J. Swift, "Physical properties of seawater," in *Descriptive Physical Oceanography* (Elsevier Ltd., 2011), pp. 29–65.
14. R. A. Cox, M. J. McCartney, and F. Culkin, "The specific gravity/salinity/temperature relationship in natural sea water," Oceanogr. Abstr. **17**(4), 679–689 (1970).
15. *Handbook of Chemistry and Physics,* D. R. Lide, ed. (CRC, 1992).
16. F. W. Kremkau, *Diagnostic Ultrasound Principles and Exercises.* (Harcourt Health Sciences Group, 1980).
17. B. Wang and S. Emelianov, "Thermal intravascular photoacoustic imaging," Biomed. Opt. Express **2**(11), 3072–3078 (2011).
18. L. Gao, L. Wang, C. Li, Y. Liu, H. Ke, C. Zhang, and L. V. Wang, "Single-cell photoacoustic thermometry," J. Biomed. Opt. **18**(2), 026003 (2013).
19. I. V. Larina, K. V. Larin, and R. O. Esenaliev, "Real-time optoacoustic monitoring of temperature in tissues," J. Phys. D Appl. Phys. **38**(15), 2633–2639 (2005).
20. J. Shah, S. Park, S. Aglyamov, T. Larson, L. Ma, K. Sokolov, K. Johnston, T. Milner, and S. Y. Emelianov, "Photoacoustic imaging and temperature measurement for photothermal cancer therapy," J. Biomed. Opt. **13**(3), 034024 (2008).
21. S. M. Nikitin, T. D. Khokhlova, and I. M. Pelivanov, "Temperature dependence of the optoacoustic transformation efficiency in ex vivo tissues for application in monitoring thermal therapies," J. Biomed. Opt. **17**(6), 061214 (2012).
22. B. Soroushian, W. M. Whelan, and M. C. Kolios, "Study of laser-induced thermoelastic deformation of native and coagulated ex-vivo bovine liver tissues for estimating their optical and thermomechanical properties," J. Biomed. Opt. **15**(6), 065002 (2010).
23. M. Pramanik and L. V. Wang, "Thermoacoustic and photoacoustic sensing of temperature," J. Biomed. Opt. **14**(5), 054024 (2009).
24. A. A. Anosov and L. R. Gavrilov, "Reconstruction of the in-depth temperature distribution for biological objects by liner phased arrays," Acoust. Phys. **51**(4), 376–384 (2005).
25. A. V. Liopo, A. Conjusteau, O. V. Chumakova, S. A. Ermilov, R. Su, and A. A. Oraevsky, "Highly purified biocompatible gold nanorods for contrasted optoacoustic imaging of small animal models," Nanosci Nanotechnol Lett **4**(7), 681–686 (2012).
26. G. P. Luke, D. Yeager, and S. Y. Emelianov, "Biomedical applications of photoacoustic imaging with exogenous contrast agents," Ann. Biomed. Eng. **40**(2), 422–437 (2012).
27. W. Bost, R. Lemor, and M. Fournelle, "Comparison of the optoacoustic signal generation efficiency of different nanoparticular contrast agents," Appl. Opt. **51**(33), 8041–8046 (2012).
28. C. Bao, N. Beziere, P. del Pino, B. Pelaz, G. Estrada, F. Tian, V. Ntziachristos, J. M. de la Fuente, and D. Cui, "Gold nanoprisms as optoacoustic signal nanoamplifiers for in vivo bioimaging of gastrointestinal cancers," Small **9**(1), 68–74 (2013).
29. S. Egerev, S. Ermilov, O. Ovchinnikov, A. Fokin, D. Guzatov, V. Klimov, A. Kanavin, and A. A. Oraevsky, "Acoustic signals generated by laser-irradiated metal nanoparticles," Appl. Opt. **48**(7), C38–C45 (2009).
30. D.-K. Yao and L. V. Wang, "Measurement of Grüneisen parameter of tissue by photoacoustic spectrometry," Proc. SPIE **8581**, 858138 (2013).
31. N. I. Odina, A. I. Korobov, D. N. Semenov, A. N. Knysh, and T. V. Ageeva, "An automated setup for investigation of anisotropy of the gruneisen parameter of solids in the temperature range 77–350 K using the photoacoustic technique," Instrum. Exp. Tech. **51**(3), 153–158 (2008).
32. A. Korobov, N. Odina, V. Chegnov, M. Chukichev, B. Enflo, C. M. Hedberg, and L. Kari, "Experimental research of Gruneisen parameter of fullerite C60 single crystal near structural phase transition at 260 K using photoacoustic technique," in *Nonlinear Acoustics—Fundamentals and Applications (ISNA 18)*, B. O. Enflo, C. M. Hedberg, and L. Kari, eds. (2008), p. CP1022.
33. J. Zalev, D. Herzog, B. Clingman, T. Miller, K. Kist, N. K. Dornbluth, B. M. McCorvey, P. Otto, S. Ermilov, V. Nadvoretsky, A. Conjusteau, R. Su, D. Tsyboulski, and A. Oraevsky, "Clinical feasibility study of combined optoacoustic and ultrasonic imaging modality providing coregistered functional and anatomical maps of breast tumors," Proc. SPIE **8223**, 82230A, 82230A-6 (2012).
34. M. P. Fronheiser, S. A. Ermilov, H. P. Brecht, A. Conjusteau, R. Su, K. Mehta, and A. A. Oraevsky, "Real-time optoacoustic monitoring and three-dimensional mapping of a human arm vasculature," J. Biomed. Opt. **15**(2), 021305 (2010).
35. V. Nadvoretskiy, S. Ermilov, H. P. Brecht, R. Su, and A. Oraevsky, "Image processing and analysis in a dual-modality optoacoustic/ultrasonic system for breast cancer diagnosis," Proc. SPIE **7899**, 789909, 789909-6 (2011).
36. J. W. Pickering, S. A. Prahl, N. van Wieringen, J. F. Beek, H. J. Sterenborg, and M. J. C. van Gemert, "Double-integrating-sphere system for measuring the optical properties of tissue," Appl. Opt. **32**(4), 399–410 (1993).
37. L. Hanssen, "Integrating-sphere system and method for absolute measurement of transmittance, reflectance, and absorptance of specular samples," Appl. Opt. **40**(19), 3196–3204 (2001).
38. A. Conjusteau, S. A. Ermilov, R. Su, H. P. Brecht, M. P. Fronheiser, and A. A. Oraevsky, "Measurement of the spectral directivity of optoacoustic and ultrasonic transducers with a laser ultrasonic source," Rev. Sci. Instrum. **80**(9), 093708 (2009).

#195773 - $15.00 USD Received 27 Aug 2013; revised 4 Oct 2013; accepted 4 Oct 2013; published 14 Oct 2013

39. G. M. Spirou, A. A. Oraevsky, I. A. Vitkin, and W. M. Whelan, "Optical and acoustic properties at 1064 nm of polyvinyl chloride-plastisol for use as a tissue phantom in biomedical optoacoustics," Phys. Med. Biol. **50**(14), N141–N153 (2005).
40. J. R. Cook, R. R. Bouchard, and S. Y. Emelianov, "Tissue-mimicking phantoms for photoacoustic and ultrasonic imaging," Biomed. Opt. Express **2**(11), 3193–3206 (2011).
41. W. Xia, D. Piras, M. Heijblom, W. Steenbergen, T. G. van Leeuwen, and S. Manohar, "Poly(vinyl alcohol) gels as photoacoustic breast phantoms revisited," J. Biomed. Opt. **16**(7), 075002 (2011).
42. J. M. Steinke and A. P. Shepherd, "Effects of temperature on optical absorbance spectra of oxy-, carboxy-, and deoxyhemoglobin," Clin. Chem. **38**(7), 1360–1364 (1992).
43. L. Cordone, A. Cupane, M. Leone, and E. Vitrano, "Optical absorption spectra of deoxy- and oxyhemoglobin in the temperature rance 300-20 K," Biophys. Chem. **24**(3), 259–275 (1986).
44. D. Theodorescu, "Cancer cryotherapy: evolution and biology," Rev. Urol. **6**(Suppl 4), S9–S19 (2004).
45. B. Rubinsky, "Cryosurgery," Annu. Rev. Biomed. Eng. **2**(1), 157–187 (2000).
46. S. B. Williams, Y. Lei, P. L. Nguyen, X. Gu, S. R. Lipsitz, H.-Y. Yu, K. J. Kowalczyk, and J. C. Hu, "Comparative effectiveness of cryotherapy vs brachytherapy for localised prostate cancer," BJU Int. **110**(2), E92–E98 (2012).
47. N. Larson, A. Gormley, N. Frazier, and H. Ghandehari, "Synergistic enhancement of cancer therapy using a combination of heat shock protein targeted HPMA copolymer-drug conjugates and gold nanorod induced hyperthermia," J. Control. Release **170**(1), 41–50 (2013).
48. G. Onik, "Image-guided prostate cryosurgery: state of the art," Cancer Contr. **8**(6), 522–531 (2001).
49. I. Y. Petrov, Y. Petrov, D. S. Prough, I. Cicenaite, D. J. Deyo, and R. O. Esenaliev, "Optoacoustic monitoring of cerebral venous blood oxygenation though intact scalp in large animals," Opt. Express **20**(4), 4159–4167 (2012).
50. T. N. Erpelding, C. Kim, M. Pramanik, L. Jankovic, K. Maslov, Z. Guo, J. A. Margenthaler, M. D. Pashley, and L. V. Wang, "Sentinel lymph nodes in the rat: noninvasive photoacoustic and US imaging with a clinical US system," Radiology **256**(1), 102–110 (2010).
51. T. Harrison and R. J. Zemp, "Coregistered photoacoustic-ultrasound imaging applied to brachytherapy," J. Biomed. Opt. **16**(8), 080502 (2011).
52. M. D. Gillett, M. T. Gettman, H. Zincke, and M. L. Blute, "Tissue ablation technologies for localized prostate cancer," Mayo Clin. Proc. **79**(12), 1547–1555 (2004).

1. Introduction

Grüneisen parameter is one of the key material components contributing to optoacoustic phenomenon, which has a variety of applications in modern science, technology, biology, and medicine from extremely sensitive detection of molecular traces to sophisticated three dimensional imaging of biological tissues and even whole organisms [1–6]. The optoacoustic effect is manifested when optical energy is rapidly deposited into an absorbing medium at rates faster than relaxation through thermal, acoustic, and other mechanisms [1,7]. Typically it is achieved by illumination with a Q-switched laser with pulse duration on the order of 1-100 ns. In this case, the accumulated mechanical stress is proportional to the local optical fluence (F), optical absorption coefficient (μ_a), and thermoelastic efficiency of the medium [7,8]. If the resultant stress (σ) has negligible shear component, than thermoelastic efficiency becomes a Grüneisen parameter of the medium (Γ) [1,7,8]. For such conditions, the amplitude of stress signals carried by travelling acoustic waves and measured by optoacoustic sensors is proportional to the Grüneisen parameter at the location of optoacoustic sources [9]:

$$\sigma \sim \xi \, \Gamma \mu_a F, \tag{1}$$

where ξ is a coefficient responsible for distortion and attenuation of propagating acoustic waves.

Grüneisen is a multicomponent parameter that incorporates volumetric thermal expansion (β), speed of sound for longitudinal waves (V_l), and – specific (per mass) heat capacity at constant pressure (C_p):

$$\Gamma = \frac{\beta V_l^2}{C_p}. \tag{2}$$

If all the components are known, Grüneisen parameter can be calculated directly. Grüneisen parameter of distilled water at room temperature is equal to 0.11 [10–12]. Due to very large heat capacity of water, the majority of other substances have higher Gruneisen

#195773 - $15.00 USD Received 27 Aug 2013; revised 4 Oct 2013; accepted 4 Oct 2013; published 14 Oct 2013

parameter. For example, 0.17 for seawater (salinity of 35 mg/ml), 0.58 for ethyl alcohol, and 0.71 for mineral oil [13–16].

In Eq. (2) all of the components on the right side are generally temperature dependent, making the Grüneisen parameter, and the whole optoacoustic response temperature dependent as well. For some liquids, this dependence is significant and linear in a certain range of temperatures. For example, Grüneisen parameter of distilled water can be linearly approximated in the range from room temperature 22°C to 4°C with zero thermoacoustic efficiency corresponding to the maximum of the water density around 4°C [15].

Knowing temperature dependence of Grüneisen parameter is extremely important, for example, in some of the emerging applications on optoacoustic temperature monitoring [17–24]. Another important application is research and development of optoacoustic contrast agents [25–28]. When a Q-switched laser pulse is absorbed by a plasmonic nanoparticle or other type of particulate optoacoustic contrast agent, the local temperatures quickly (in several nanoseconds) change by tens of degrees [29]. In order to understand and being able to correctly predict the physics of the photoacoustic phenomenon in this case a good knowledge of Grüneisen parameter as a function of temperature is required.

For most solid materials, fluids, and live tissues, there isn't sufficient information on temperature dependence of Grüneisen parameter or its components. Addition of solute, such as salt or protein, changes physical properties of solution to become sometimes very different from those of water. Bodily fluids such as blood or lymph have complex composition and are even more different from water than saline. There were attempts to estimate Grüneisen parameter of biological tissues using optoacoustic sensing [22,30]. However, authors reported the high susceptibility of their measurements to noise prevented them from finding a difference in the Grüneisen parameter of native and coagulated bovine liver tissues [22]. Optoacoustic spectroscopy can reach high accuracy (about 6%) in measuring Grüneisen parameter, but requires acquisition of large amount of data. The Grüneisen parameter of porcine fat tissue and bovine red blood cells was estimated only at room temperature [30]. It makes potential temperature monitoring complicated and expensive. Other researchers performed optoacoustic measurements of anisotropy of Grüneisen parameter as a function of temperature (77-350 K) in solid materials such as strontium titanate, triglycine sulfate [31], and fullerite C60 [32] single crystals. But the technique could not be applied to soft biomaterials and liquid samples. Very limited amount of data and developing optoacoustic applications on temperature monitoring demand for a reliable technique for measurements of the temperature dependence of Grüneisen parameter.

In this work we present and validate a novel methodology for accurate measurements of temperature dependence of Grüneisen parameter for optically absorbing liquids. High accuracy is achieved due to improved signal-to-noise ratio and sensitivity, as well as accurate localization of the samples attainable via two-dimensional optoacoustic imaging. Also, multiple samples could be simultaneously studied, which increases the data throughput. By normalizing optoacoustic data to a particular temperature, we confine systematic errors caused by spatial fluctuations of fluence and optical absorption, as well as distortions of propagating optoacoustic waves. We demonstrate the performance of our technique by estimating temperature dependence of Grüneisen parameter for different concentrations of pentahydrate cupric sulfate in a range of temperatures (from 22 to 4°C) important in future applications of optoacoustic imaging for live monitoring of tissue hypothermia prior to freezing.

2. Equipment and materials

Our setup utilizes a 128-channel real-time (up to 10 frames per second, 40 MHz sampling rate) two-dimensional laser optoacoustic imaging system (LOIS, TomoWave Laboratories, Houston TX) with a linear acoustic probe, which was previously developed by our company for breast imaging [33]. The system also demonstrated good performance in imaging of solid

#195773 - $15.00 USD Received 27 Aug 2013; revised 4 Oct 2013; accepted 4 Oct 2013; published 14 Oct 2013

and liquid tissue phantoms and peripheral vasculature [34,35]. Ti-Sapphire output of the laser unit (Spectra Wave, TomoWave Laboratories, Houston, TX) was tuned to 800 nm and produced 6 ns, 28 mJ per pulse laser radiation with pulse repetition rate of 10 Hz. Light was delivered to the samples by two randomized optical fiber bundles terminated in rectangular output apertures (1.5 mm x 50 mm each), producing laser fluence about 3 mJ/cm^2 at 20 mm depth. The light bars were attached on both sides of the ultrasonic array forming a backward optoacoustic illumination mode. The probe and fiberoptic outputs were hermetically sealed to enable operation in liquid environment.

Our test unit contained four tubes filled with sample solutions. Two pairs were located at depths of 17 and 26 mm from the linear ultrasound probe. The tubes were positioned orthogonally to the imaging plane, so that their cross-sections could be observed on reconstructed optoacoustic images. PTFE tubes (Sub-Lite-Wall Tubing, Zeus, Orangeburg, SC) of inner diameter 0.635 mm and wall thickness 0.051 mm were filled with aqueous solution of $CuSO_4 \cdot 5H_2O$ (99% pure salt), having molar absorptivity of $\varepsilon = 10.57 \pm 0.13$ $M^{-1}cm^{-1}$ at 800 nm as measured by spectrophotometer (Evolution 201, Thermo Scientific, Waltham, MA). We performed experiments using 6 concentrations of cupric sulfate pentahydrate solution: 12, 60, 120, 240, 360, and 480 mM. We selected pentahydrate cupric sulfate as an optically absorbing compound with relatively high absorbance in the near-infrared range and low molecular weight, allowing for studies of diluted aqueous solutions. It was also expected that structural and optical properties of this compound would not be affected at wide range of temperatures. To estimate optical absorption as a function of temperature we preheated or precooled a sealed cuvette with a sample solution in a water bath, measured optical absorption with spectrophotometer, and acquired temperature data immediately after taking optical spectra.

We employed a chest freezer (CF-1510, Avanti, Miami, FL) for cooling of a thermostat tank. The 1.5 L tank was filled with distilled water and was subject to 0.2 °C/min cooling rate. The temperature was measured and logged by digital thermometer (HH806AU, Omega, Stamford, CT) with precision of 0.1°C. When fine gauge thermocouples were placed both inside and outside of the tubes, we found that their temperature readings were systematically different by 0.2°C, which was in agreement with the required precision of measurements. Therefore, in experiments we used temperature readings from the thermocouple, which was located in the proximity (5 mm), but outside of the sample tubes.

3. Methods

The schematics of experimental setup is depicted in Fig. 1(a) and a photograph showing the probe (1), fiberoptic light bars (2), and sample tubes (3) assembled within a rigid bracket is shown in Fig. 1(b). Fiberoptic illuminators were adjusted to maximize fluence in the imaging plane of the probe at the level of sample tubes. Size of the probe and the established illumination pattern allowed to reconstruct image of total size 38×38 mm^2. The recorded optoacoustic and temperature data were time stamped with respect to the internal PC clock for subsequent synchronization.

#195773 - $15.00 USD Received 27 Aug 2013; revised 4 Oct 2013; accepted 4 Oct 2013; published 14 Oct 2013

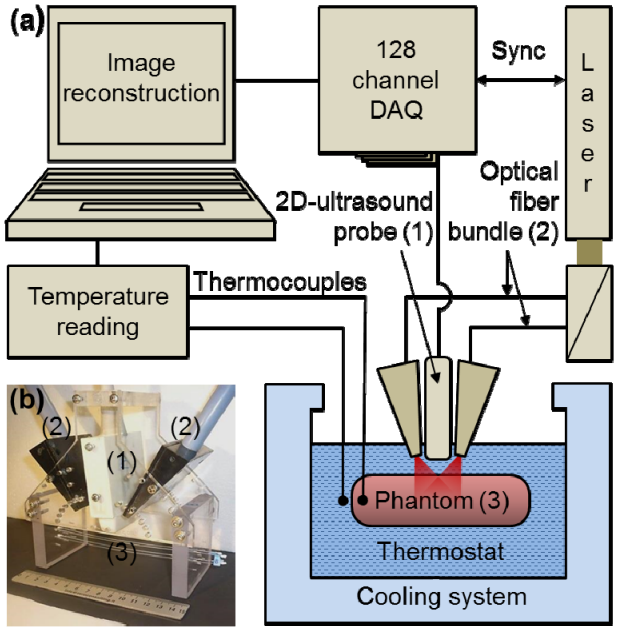

Fig. 1. (a) Schematics of the experimental setup. (b) Photograph showing the optoacoustic probe (1), the light bars (2) and the tubes filled with samples (3) integrated via a rigid acrylic bracket. The ruler shown in front of the bracket is 15 cm long.

Prior to each experiment, we performed test imaging at room temperature and adjusted the amplification of DAQ module for the best image contrast of the samples. We acquired optoacoustic images of the samples every 10 s while temperature was slowly decreased from 22 to 4 °C. At lower temperatures ice crystals spontaneously nucleated in thermostat bath and did not allow us to continue accurate measurements. Temperature was recorded every 5 s. The same computer was used to record both optoacoustic and temperature data, allowing post-experiment synchronization via a timestamp from the PC clock. The implemented synchronization procedure produced only insignificant decrease in accuracy of temperature measurements, by no more than ± 0.025 °C.

Each optoacoustic frame was reconstructed using 2D filtered backprojection of measured integrated signals. To increase SNR and remove low-frequency optoacoustic artifacts manifested in the background, we performed digital post processing of optoacoustic signals with zero-phase infinite impulse response bandpass filter (1-5 MHz sixth order Butterworth) using built-in *filtfilt* function in Matlab (Mathworks, Natick, MA). The filter was preferred over its second order counterpart due to better artifact removal performance. It also bested its tenth order analogue due to smaller amplitude of introduced post-filter ringing. Since optoacoustic signals generated by 0.635 mm tubes have the main lobe of their spectrum within the bandwidth of utilized probe (1.5-6 MHz at −6dB), the detected waveforms preserved their original N-shaped form, and it was not necessary to perform deconvolution of the probe's impulse response.

Figure 2(a) shows a reconstructed image of four tubes' cross-sections (bright images on gray background). The square indicates area selected for analysis around the tube with the lowest concentration of sample cupric sulfate. Autoscaling within the selected area allowed high-contrast imaging even for samples with the lowest concentration of optically absorbing solution [Fig. 2(b)]. The processed signal profile on the right inset of the Fig. 2(b) corresponds to the central channel of the probe. It clearly shows optoacoustic signal generated

#195773 - $15.00 USD Received 27 Aug 2013; revised 4 Oct 2013; accepted 4 Oct 2013; published 14 Oct 2013

by the pair of tubes closest to the probe (about 17 mm deep) with background effectively removed by filtering. However, signals measured by a single transducer do not allow one to resolve individual tubes within the pair. It only becomes possible by collecting data from multiple transducers and using tomography to reconstruct the image with all four tubes clearly visible [Fig. 2(a)]. Figures 2(b)-2(d) illustrate temperature dependence of optoacoustic image intensity for the tube filled with 12 mM of aqueous cupric sulfate ($\mu_a \approx 0.29$ cm^{-1}). The image frame taken at 12°C was selected as a reference for dynamic range freeze procedure, which allows qualitative visual comparison of intensities in multiple frames and/or movies. It is obvious that at 20°C image of the tube cross-section is much brighter than the one at 6°C. To obtain a quantitative metric of the optoacoustic response, we evaluated the median intensity inside a region of interest (ROI) manually selected on the first reconstructed frame of the tube cross-section and shown as a dashed circle inside the bright area in Fig. 2(b). The circle has a diameter of 0.4 mm, which is less than the inner diameter of a tube. Therefore, the selected ROI contains information on optoacoustic response only from the sample solution. Using median estimate of the optoacoustic image intensity made our measurements less sensitive to the ROI tracking.

The important part of the imaging procedure is the continuous speed of sound adjustment, which significantly changes with temperature. If speed of sound is kept constant in reconstruction, the tube image gets distorted and moves beyond the boundary of measurements (see top right insets on Figs. 2(b) and 2(c)). In our experiments, the speed of sound was automatically adjusted for each frame using its known dependence on temperature for aqueous background [10].

#195773 - $15.00 USD Received 27 Aug 2013; revised 4 Oct 2013; accepted 4 Oct 2013; published 14 Oct 2013

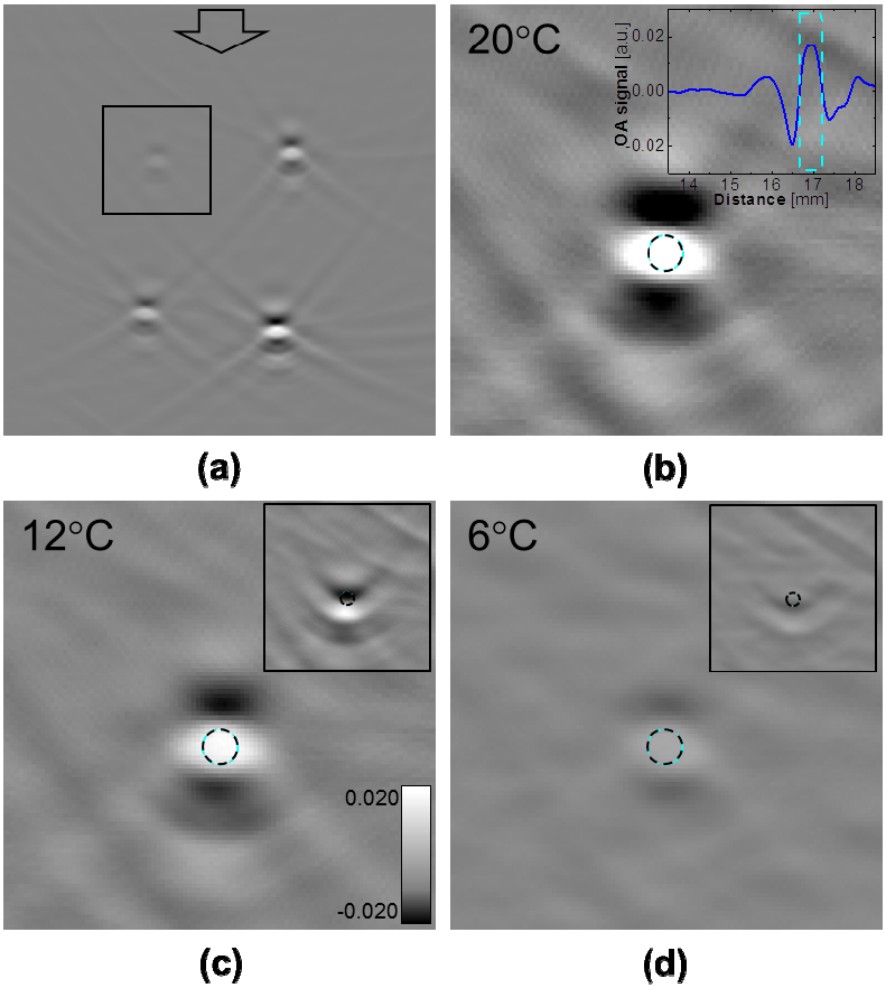

Fig. 2. (a) 20 × 20 mm^2 two dimensional optoacoustic image showing 4 sample tubes filled with aqueous solutions of $CuSO_4 \cdot 5H_2O$: top left – 12 mM, top right and lower left – 60 mM, lower right – 120 mM. Linear grayscale palette is extended over the full dynamic range. The top pair of tubes is located 17 mm from the transducer array, the second pair – about 25 mm. Square indicates a 5 × 5 mm^2 area around the top left sample, which is magnified and presented on subsequent panels. Arrow indicates direction of illumination and location of the central probe element. (b-d) 2D optoacoustic images of a tube with 12 mM aqueous solution of $CuSO_4 \cdot 5H_2O$. Images were acquired at temperatures indicated on each panel. Tube has an inner diameter of 0.635 mm and wall thickness of 0.051 mm. The selected ROI is a 0.4 mm diameter dashed circle. For direct visual comparison the images are shown in gray palette linearly scaled over the full dynamic range of the frame acquired at 12°C. The colorbar with the corresponding dynamic range is shown on panel (c). Data displayed on the panel (b) has full dynamic range [-0.040 ÷ 0.040] and the image colors are saturated for pixels with intensities below –0.020 and above 0.020. Data on panel (d) has full dynamic range [-0.006 ÷ 0.006] and, therefore, is mapped to the gray portion of the image palette. Speed of sound for background water bath is varied in reconstruction according to the temperature: (b) 1485 m/s; (c) 1455 m/s; (d) 1430 m/s. Top right corner insets on Panels (c) and (d) illustrate distorted images resulting from an optoacoustic reconstruction assuming constant speed of sound of 1485 m/s. Top right corner inset on Panel (b) shows a portion of the optoacoustic signal corresponding to the closest pair of tubes as it is registered by the central channel.

Eventually, the median intensity of each tube cross section was plotted for all the frames as a function of time and temperature.

#195773 - $15.00 USD Received 27 Aug 2013; revised 4 Oct 2013; accepted 4 Oct 2013; published 14 Oct 2013

4. Results

The top right and lower left tubes on Fig. 2(a) were filled with the same 60 mM solution of $CuSO_4 \cdot 5H_2O$. Due to divergence of the laser illumination, the tubes experienced different fluence resulting in higher optoacoustic response of the top sample, which was situated closer to the optoacoustic probe. The difference in measured optoacoustic response was further amplified by increased acoustic diffraction and attenuation for the more distant sample. Figure 3(a) illustrates time dependence of optoacoustic median intensity measured for those two samples upon their cooling. The inset shows the temporal temperature profile coregistered with the optoacoustic imaging. It can be noticed that for both samples, optoacoustic intensity changes about 5 times during the experiment. Therefore, we proposed that being normalized to the intensity at a particular temperature, for example $T_n = 20°C$, both graphs will coincide. The reasoning becomes clear if we look at the Eq. (1) and assume that the fluence, optical absorption, and the acoustic distortion coefficient are invariant or change insignificantly with temperature. Then the normalized optoacoustic intensity will represent the normalized Grüneisen parameter, which is the objective of our studies:

$$\bar{I}_n(T) = \frac{I(T)}{I(T_n)} = \frac{\Gamma(T)}{\Gamma(T_n)}. \tag{3}$$

The plot of normalized optoacoustic intensity as a function of temperature results in two straight lines perfectly coinciding for both samples [Fig. 3(b)], which demonstrates that our technique is not sensitive to the local fluence and distortions of the propagating optoacoustic waves.

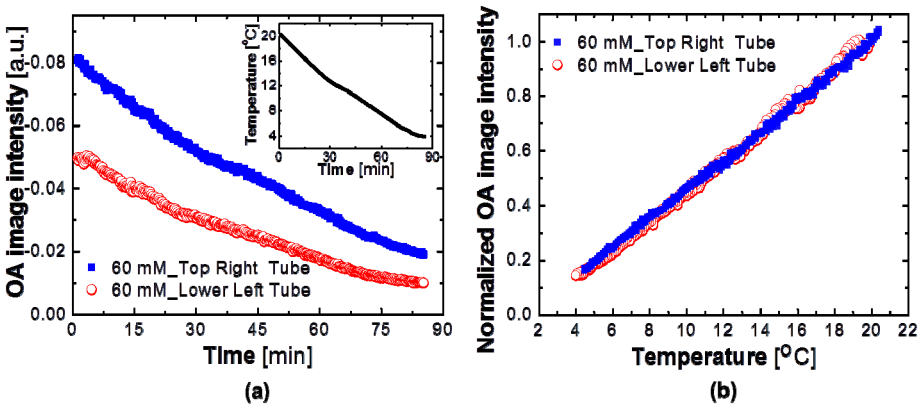

Fig. 3. Analysis of optoacoustic images for two 60 mM $CuSO_4 \cdot 5H_2O$ samples experiencing different local optical fluence and distortion of propagating optoacoustic waves. (a) Temporal profiles of the measured median optoacoustic intensity during cooling of the samples from 22 to 4°C. Temporal profile of the corresponding temperature change is depicted on the inset. (b) Optoacoustic intensity normalized to 20°C as a function of temperature.

To validate that the changes of optoacoustic response that we observed with temperature were not caused by the changes of optical absorption of the samples, we measured optical absorption spectra of few samples at different temperatures. We selected concentrations of cupric sulfate solution which were in the range of spectrophotometer sensitivity at 800 nm. Optical absorption spectra of 60 mM $CuSO_4 \cdot 5H_2O$ as well as distilled water measured at different temperatures are presented in Fig. 4(a). Optical absorption of distilled water at 22°C served as a reference in all the cases. Spectral profiles look similar without any signature peak shifts. At the wavelength of optoacoustic measurements (800 nm) water does not affect absorbance of solution. We found that optical absorption of $CuSO_4 \cdot 5H_2O$ at 800 nm linearly

#195773 - $15.00 USD Received 27 Aug 2013; revised 4 Oct 2013; accepted 4 Oct 2013; published 14 Oct 2013

changes with temperature and the slope increases for more concentrated solutions [Fig. 4(b)]. We estimated that for 40, 60, and 120 mM solutions the absorbance slope dA/dT was about 2.2×10^{-3}, 3.3×10^{-3}, and 6.9×10^{-3} K^{-1}, respectively. However, fractional increase of optical absorption in the studied temperature range (4 – 22°C) was less than 10% for the most concentrated (120 mM) solution of cupric sulfate, which is negligible in comparison to overall 500% growth of optoacoustic signals. Therefore, it was safe to assume that our technique, indeed, allowed accurate measurements of thermal changes of Grüneisen parameter in the studied samples.

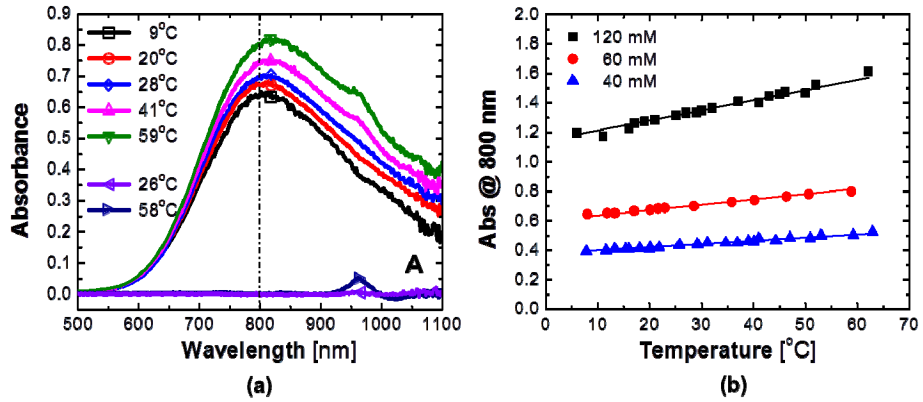

Fig. 4. (a) Optical absorption spectra of aqueous solution of $CuSO_4 \cdot 5H_2O$ (60 mM) measured at different temperatures (5 top curves). Optical absorption spectra of distilled water are shown at 26°C and 58°C as the two lower profiles. All the spectra were measured with a reference to distilled water at 22°C. (b) Optical absorbance at 800 nm as a function of temperature for three concentrations of $CuSO_4 \cdot 5H_2O$. The estimated extinction coefficient at 0°C is $\varepsilon_0 = 9.38 \pm 0.24$ $M^{-1}cm^{-1}$, which is about 11% decrease from its value at room temperature.

To validate our technique and demonstrate its utility for measurements of thermal changes of Grüneisen parameter, we performed experiments using 6 concentrations of $CuSO_4 \cdot 5H_2O$ from 12 to 480 mM (2-4 samples per each concentration). Temperature relationships of the normalized optoacoustic intensity are shown for some individual samples in Fig. 5(a). All the plots have linear dependence on temperature, and the relationship for the smallest studied concentration of cupric sulfate coincide with the thermal changes of Grüneisen parameter for pure water, which can be calculated using temperature dependent data of speed of sound [10], isotropic thermal expansion [12], and heat capacity at constant pressure [11].

#195773 - $15.00 USD Received 27 Aug 2013; revised 4 Oct 2013; accepted 4 Oct 2013; published 14 Oct 2013

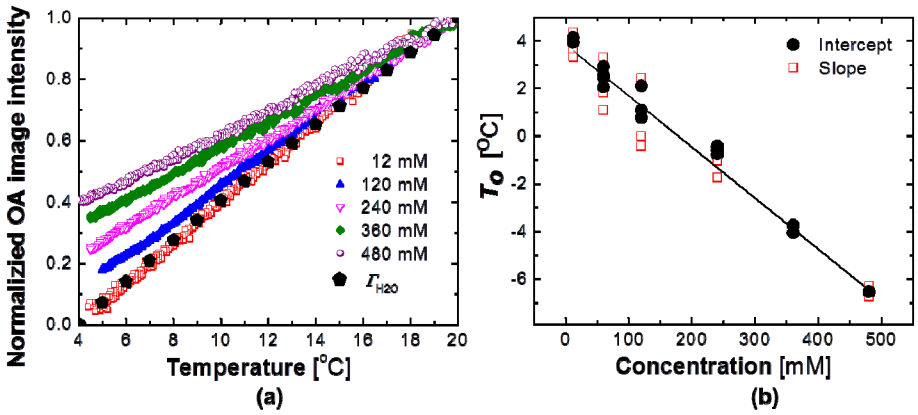

Fig. 5. (a) Normalized optoacoustic intensity as a function of temperature for different concentrations of $CuSO_4 \cdot 5H_2O$. Grüneisen parameter of water (Γ_{H2O}) was calculated for each degree and presented after normalization at T_n = 20°C. (b) Scatter plot and its linear fit for the parameter T_0 as a function of concentration estimated from the data slope (opened squares) and intercept (solid circles).

Linear relationship between Grüneisen parameter of cupric sulfate solution and temperature in the range of 4 – 22°C could be represented by the following equation:

$$\Gamma(c,T) = \frac{\partial \Gamma}{\partial T}(c) \cdot (T - T_0(c)), \tag{4}$$

where c is the molar concentration of solution (mM), T is the temperature (°C), and T_0 indicates the temperature where Grüneisen parameter would become zero. In such a special case when Grüneisen parameter changes linearly with temperature, our metric (normalized optoacoustic intensity) becomes insensitive even to the thermal changes of Grüneisen parameter ($\partial\Gamma/\partial T$), and will only depend on the temperature T, T_n and T_0:

$$\bar{I}_n(c,T) = \frac{T - T_0(c)}{T_n - T_0(c)} = a_0(c) + a_1(c) \cdot T. \tag{5}$$

Then material-specific parameter T_0 can be estimated as a function of concentration of $CuSO_4$ solution using either slope (a_1) or intercept (a_0) in the relationship (5):

$$T_0(c) = T_n - \frac{1}{a_1(c)}, \tag{6}$$

$$T_0(c) = \frac{a_0(c) \cdot T_n}{a_0(c) - 1}. \tag{7}$$

Figure 5(b) shows T_0(c) relationship for the pentahydrate cupric sulfate estimated from Eq. (6) and (7), both being in good agreement.

5. Discussion

General difficulties in estimating Grüneisen parameter are associated with its multicomponent nature providing no means for direct measurement. One must accurately obtain all three contributing physical characteristics: speed of sound, specific heat capacity at constant pressure, and volumetric thermal expansion. It is possible, although inconvenient, when a measurement at a single temperature is required. However, if the objective is the thermal

#195773 - $15.00 USD Received 27 Aug 2013; revised 4 Oct 2013; accepted 4 Oct 2013; published 14 Oct 2013

dependence of Grüneisen parameter, that type of measurements becomes extremely difficult to carry out. In that case, measuring optoacoustic response to quantify temperature changes of Grüneisen parameter has a definite advantage. In most of the situations it will require a single type of experiment, which would correlate accurately measured optoacoustic response to controlled temperature of the sample. Physical characteristics other than Grüneisen parameter, which also contribute to optoacoustic response [Eq. (1)] often remain constant in a wide range of temperatures, and if necessary could be accurately evaluated for a particular setup. Optical absorption of a sample could be measured with spectrophotometer, or integrating sphere in case of significant scattering [36,37]. Local fluence could be calibrated prior to inserting a sample with an energy meter, modified to work in the experimental liquid environment and able to provide fine 0.5-1 mm spatial sampling. Finally, the distortion of optoacoustic waves and absolute calibration of the DAQ could be performed by measuring response from optoacoustic sample located at different distances from a transducer and by using a calibrated hydrophone, respectively [38].

In these studies we demonstrated that normalized optoacoustic intensity is a reliable parameter that can be used for evaluation of temperature changes of Grüneisen parameter and is minimally or not sensitive to the other factors contributing to the optoacoustic response [Fig. 3]. Excellent correspondence between normalized optoacoustic intensity for low-concentrated salt and normalized Grüneisen parameter of water [Fig. 5(a)] provides strong evidence that the described method can be used in measurements of Grüneisen parameter of different liquid solutions. If the value of Grüneisen parameter is known at a single temperature then the presented technique can provide absolute calibration of Grüneisen parameter at other temperatures. The methodology can also be used to investigate gels and other similar materials, for example, gelatin and polyvinyl chloride plastisol (PVCP), which are conveniently used to build phantoms for development and calibration of optoacoustic imaging systems [39–41].

The proposed methodology is using 2D optoacoustic imaging and is significantly more robust, sensitive, and convenient, than using optoacoustic sensing with a single transducer. As it was shown in Fig. 2, optoacoustic signals from samples could be difficult to identify, while collecting data from large number of transducers with subsequent tomographic reconstruction increases both SNR and fidelity of the identified ROI. Residual plots in Fig. 6 demonstrate precision achieved by normalized 2D imaging versus normalized signals from transducer number 96, which was the closest to one of our samples (12 mM $CuSO_4$) and allowed its best identification. In the case of 2D imaging the residual sum of squares (RSS) is about 0.3, whereas in case of normalized optoacoustic signal RSS is 11.7, which is noticeable from much greater noise introduced by a single-transducer measurements. That noise represents single measurement errors and is accordingly translated into the errors of the model fit. Since the stochastic noise is significantly reduced during image formation, deterministic component of optoacoustic imaging artifacts becomes a key factor limiting the applicability of our technique for low-absorbing objects.

#195773 - $15.00 USD Received 27 Aug 2013; revised 4 Oct 2013; accepted 4 Oct 2013; published 14 Oct 2013

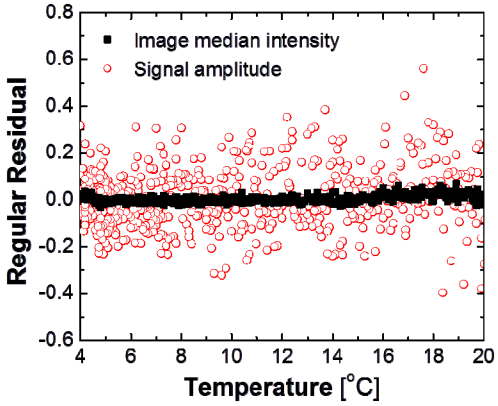

Fig. 6. Residuals of the linear regression models that were used to fit normalized optoacoustic intensity (solid squares) and normalized optoacoustic signals from channel number 96 (opened circles) showing the precision of the Grüneisen estimation using both techniques. Imaging: Residual sum of squares (RSS) – 0.3, R-Square – 0.998, adjusted R-Square – 0.996; Sensing: RSS - 11.7, R-Square – 0.924, adjusted R-Square – 0.854.

If optoacoustic sensing system can time-resolve N individual samples then an optoacoustic array composed of the same transducers can simultaneously measure $N \cdot W/(r + d)$ samples, where W – field of view width, r is the lateral resolution of the array, and d is the diameter of the sample. Typically a 40 mm wide field of view could be easily achieved in an optoacoustic imaging system equipped with a standard ultrasound probe for general clinical applications, similar to the one we used in these studies. In our case, lateral resolution at the depth of 25 mm is approximately 1 mm considering widening of 0.635 mm tube cross-sections as it could be estimated from Fig. 2(a). Therefore, we should be able to perform optoacoustic imaging with tube centers laterally separated by 1.7 mm. The productivity in that case of multi-sample experiments could be increased more than 20 times as compared to the sensing-based technique.

When using optoacoustic imaging technique to estimate thermal changes of Grüneisen parameter, careful consideration of changes in local optical absorption must be taken. Cupric sulfate did show a change in its optical absorption with temperature at 800 nm, but those changes were about 2% the magnitude of the changes of measured optoacoustic response, and could be rightfully neglected. However, some other substances, especially proteins may change their optical absorption more dramatically with temperature. One particular example is hemoglobin, which is a primary optical absorber and plays the major role during *in vivo* optoacoustic imaging and temperature monitoring. It was reported that optical absorption of hemoglobin slightly decreases (by 10%) in visible and near-infrared parts of spectra under soft heating 20 – 40°C [42] and significantly increases (by 160%) during deep freezing from 25 to –253°C [43]. It was shown that hemoglobin denaturation and degradation affect optoacoustic response from tissues by doubling the signal amplitude mostly due to transformation of optical absorbance spectra at 45 – 75°C [21,22]. In that case, our technique will yield reduced accuracy unless the changes in optical absorption are directly accounted for. Our technique is also applicable for studies of optically scattering media – both sample and background. In that case, it is much more difficult to accurately measure optical absorption and local fluence. The proposed methodology will still work well as long as thermal changes of Grüneisen parameter are of interest rather than its absolute value. That feature of our technique is particularly important for future applications in live tissues, which have significant optical scattering component.

#195773 - $15.00 USD Received 27 Aug 2013; revised 4 Oct 2013; accepted 4 Oct 2013; published 14 Oct 2013

Using our technique we were able to obtain detailed information on behavior of Grüneisen parameter at different temperatures for multiple concentrations of cupric sulfate. All the temperature profiles showed excellent linear trend [Fig. 5(a)]. It is known that Grüneisen parameter of pure water has linear dependence on temperature in the studied range of 4 - 22°C and becomes zero at T_0 ≈4°C, where the water has maximum density and zero volumetric thermal expansion coefficient [15]. Our measured normalized optoacoustic intensity for the most diluted solution of cupric sulfate (12 mM) accurately followed the normalized Grüneisen parameter of water with an estimated T_0 = 3.8°C. While we increased concentration of cupric sulfate, T_0 shifted towards more negative temperatures, reaching −6.5°C for 480 mM solution. Usually, salt solutions have decreased temperatures at which maximum density is reached, which would explain the concentration dependent behavior of T_0 observed for cupric sulfate. Our samples had concentrations between 3 and 120 mg/ml. In comparison seawater or aqueous sodium chloride has maximum density at 2°C for salinity about 8 mg/ml, 0°C for 18 mg/ml, and −2°C for 27 mg/ml [13].

It is important to mention how the developed method could be adopted to advance emerging applications of optoacoustic temperature monitoring during thermal therapy when biological tissues are selectively heated or cooled to create local therapeutic effect in pathological conditions like cancer and arrhythmia [44–47]. As it became evident, reconstruction of temperature maps would require: taking into account changes of speed of sound in the background medium [Fig. 2], appropriate statistical estimate of the local optoacoustic intensity (in our studies median value measured within the selected ROI was proposed since it is not sensitive to outliers), and normalization to optoacoustic intensity measured at the known local temperature, for example, local tissue temperature prior to thermal therapy. For accurate temperature monitoring it is also important to perform measurements in the linear mode, which for Grüneisen parameter and the proposed normalized optoacoustic intensity would involve limited temperature range. For example, Grüneisen parameter of water exhibits good linearity between 4 and 22°C as we showed above. In this study we used a temperature range below normal physiological 37°C, which is important for clinical applications involving monitoring of tissue hypothermia prior to freezing [48]. However, additional studies are required to find the range of actual Grüneisen linearity for physiologically relevant solutions and tissues. It is practically impossible to use optoacoustic sensing for in vivo temperature monitoring, since biological structures could be rarely identified from individual transducer signals. Only large, stand-alone blood vessels were previously monitored using single-channel optoacoustic sensing [49]. Also, often 2D temperature mapping is necessary [48], and numerous advantages including anatomical mapping, improved image quality and diagnostics could be achieved by coregistered optoacoustic and ultrasound imaging [33,50,51]. In future studies of hypothermia, lower temperatures could be achieved without freezing of the acoustic coupling medium by using thermostat bath filled with alcohol or saline.

In conclusion, here we proposed a new experimental approach for measurements of temperature dependence of Grüneisen parameter in optically absorbing solutions. The method employs normalized two-dimensional optoacoustic imaging and allows to exclude uncertainty introduced by laser fluence, optical absorption of the sample, and distortions of the propagating optoacoustic waves. Method showed to be much more effective than that using single-transducer optoacoustic sensing. Our measured data showed strong linear correlation with local temperatures for aqueous cupric sulfate in the temperature range 4 - 22°C. In future, the developed method could be adopted for important applications of in vivo optoacoustic temperature monitoring.

Acknowledgment

This work was sponsored in part by National Institutes of Health (National Cancer Institute) grant R44 CA128196.

#195773 - $15.00 USD Received 27 Aug 2013; revised 4 Oct 2013; accepted 4 Oct 2013; published 14 Oct 2013